Intrinsically disordered regions contribute promiscuous interactions to RNP granule assembly

David S. W. Protter[1], Bhalchandra S. Rao[1], Briana Van Treeck[1], Yuan Lin[2], Laura Mizoue[1], Michael K. Rosen[2] and Roy Parker[1]

Department of Chemistry and Biochemistry, Howard Hughes Medical Institute, University of Colorado, Boulder, Colorado 80309, USA

Department of Biophysics, Howard Hughes Medical Institute, University of Texas Southwestern Medical Center, Dallas, Texas 75390, USA

Correspondence/Lead Author: roy.parker@colorado.edu (R. Parker)

Abstract

Eukaryotic cells contain large RNA-protein assemblies referred to as RNP granules, whose assembly is promoted by both traditional protein interactions and intrinsically disordered protein domains. Using RNP granules as an example, we provide evidence for an assembly mechanism of large cellular structures wherein specific protein-protein or protein-RNA interactions act together with promiscuous interactions of intrinsically disordered regions (IDRs). This synergistic assembly mechanism illuminates RNP granule assembly, and explains why many components of RNP granules, and other large dynamic assemblies, contain IDRs linked to specific protein-protein or protein-RNA interaction modules. We suggest assemblies based on combinations of specific interactions and promiscuous IDRs are common features of eukaryotic cells.

INTRODUCTION

Eukaryotic cells contain a variety of non-membrane bound RNA-protein assemblies, collectively referred to as RNP granules. Such RNP granules include the nucleolus and Cajal body in the nucleus, as well as stress granules and P-bodies in the cytosol (Spector, 2006). RNP granules are generally highly dynamic, as judged by FRAP of their protein components, and exhibit liquid-like behaviors, such as flowing, fusing, and rapid reorganization of internal components (Brangwynne, 2013; Brangwynne et al., 2009). RNP granules are thought to assemble through a process referred to as liquid-liquid phase separation (LLPS) wherein RNA molecules provide binding sites for RNA binding proteins that interact with themselves or other RNA binding proteins to create a larger multivalent assembly (Elbaum-Garfinkle et al., 2015; Feric et al., 2016; Kaiser et al., 2008; Mitrea et al., 2016; Nott et al., 2015; Pak et al., 2016; Patel et al., 2015; Riback et al., 2017; Weber and Brangwynne, 2012; Zhang et al., 2015). Some of the interactions that drive RNP granule assembly are well defined interactions between folded proteins, or folded protein domains and short linear motifs (SLiMs) (Decker et al., 2007; Jonas and Izaurralde, 2013; Kedersha et al., 2016; Ling et al., 2008; Mitrea et al., 2016; Tourriere, 2003). Since these interactions require folded protein structures and/or extended linear motifs that interact in a stereospecific manner, we refer to these interactions as specific interactions.

The IDRs of RNA binding proteins have been highlighted as drivers of RNP granule assembly for three reasons. First, genetics indicate that IDRs can be important for assembly of RNP granules or localization of granule components (Decker et al., 2007; Feric et al., 2016; Gilks et al., 2004; Hennig et al., 2015; Kato et al., 2012). Second, RNP granules are often enriched in

proteins with IDRs (Decker et al., 2007; Jain et al., 2016; Kato et al., 2012; Kedersha et al., 2013; Reijns et al., 2008). Finally, IDRs are often (but not always) both necessary and/or sufficient for LLPS of granule proteins *in vitro*, forming structures that resemble RNP granules *in vivo* - (Elbaum-Garfinkle et al., 2015; Lin et al., 2015; Molliex et al., 2015; Nott et al., 2015; Patel et al., 2015; Smith et al., 2016; Zhang et al., 2015).

An unresolved issue is how IDRs contribute to RNP granule assembly, and how IDR based assembly mechanisms integrate with specific protein-protein and protein-RNA interactions to promote RNP granule formation. The literature suggests three non-mutually exclusive models by which IDRs could contribute to LLPS *in vitro* and RNP granule formation *in vivo*. First, some experiments *in vitro* suggest that IDRs promote LLPS via weak binding, utilizing electrostatic, cation-π, dipole-dipole and π-π stacking interactions (Brangwynne et al., 2015; Lin et al., 2016; Nott et al., 2015; Pak et al., 2016). Charge patterning also appears to play an important role, wherein like-charged amino acids are clustered together within an IDR. Scrambling these charges across the length of an IDR has been observed to impair LLPS both *in vitro* and *in vivo* (Nott et al., 2015; Pak et al., 2016). Because these interactions only require a few amino acids, and do not require any stereospecific arrangement, they would be anticipated to occur between an IDR and many other proteins, including other IDRs. Indeed, charge patterning specifically has been proposed to mediate interactions between IDRs and cellular proteins (Pak et al., 2016). For this reason, we refer to the above types of IDR interactions as nonspecific. These interactions will also be promiscuous, because they will be relatively indiscriminate with respect to binding partners. A second possibility is that elements within

some IDRs interact in a specific manner involving local regions of secondary structure. For example, there is a correlation with how mutations in hnRNPA2 affect binding of its C-terminal disordered domain to beta-strand rich hydrogels, and the recruitment of those hnRNPA2 domain variants to LLPS of wild-type hnRNPA2 (Xiang et al., 2015). Similarly, a locally formed α-helix in TDP-43 can mediate LLPS through homotypic interactions (Conicella et al., 2016). Finally, it is likely that a subset of IDRs are also promiscuous RNA binding proteins since they can be rich in positive charges, some IDRs can cross link to mRNA *in vivo* , and some IDRs can bind RNA *in vitro* (Lin et al., 2015; Lyons et al., 2014; Mayeda et al., 1994; Molliex et al., 2015).

Given the promiscuous nature of IDR interactions, we hypothesized that such IDR based interactions alone would be susceptible to other highly abundant proteins in cells, and therefore insufficient to drive LLPS and the assembly of an RNP granule *in vivo*. In the context of the protein-rich cellular environment other proteins would compete for binding to the IDRs and thereby prevent their forming a defined assembly. Moreover, even the ability of some IDRs to form specific local structure based interactions might be impaired by competition with other proteins in the cell. Instead, to account for the contributions from both IDRs and specific interactions to RNP granule assembly, we hypothesized that IDRs would reinforce assemblies that contained specific assembly interactions. Effectively, specific interactions would concentrate the IDRs and strengthen their interactions through additive binding energies (Jencks, 1981), either biasing their promiscuous interactions toward components of the assembly, or promoting the formation of specific interactions between the IDRs. In this way, IDR-based interactions could contribute to the energetics of assembly.

Here we provide several observations that RNP granule assembly gains selectivity from specific protein-protein and protein-RNA interactions, and that promiscuous binding of IDRs to proteins and possibly RNA enhances these assemblies. First, we observe that LLPS driven by IDRs *in vitro* is inhibited by other proteins. Second, in cells we observe that IDRs of granule components are often neither required nor sufficient to target proteins to RNP granules. Third, we demonstrate that *in vitro* LLPS driven by specific protein-RNA interactions is enhanced by adding promiscuously interacting IDRs, and the assembly of yeast P-bodies in cells is promoted by nonspecific IDRs in conjunction with specific interactions. Thus, RNP granules assemble primarily by specific interactions, which can be enhanced by IDRs capable of either promiscuous, or weak specific interactions based on small structural elements that become effective at high local concentrations. We suggest that this general assembly mechanism may be shared by other macromolecular complexes rich in IDRs.

RESULTS

Several proteins inhibit LLPS driven by IDRs *in vitro*

We hypothesized that IDRs of RNA binding proteins might not be sufficient to drive LLPS in the presence of other proteins similar to the intracellular environment, despite the observation that such IDRs are capable of undergoing LLPS as purified proteins (Elbaum-Garfinkle et al., 2015; Lin et al., 2015; Molliex et al., 2015; Nott et al., 2015; Patel et al., 2015; Smith et al., 2016; Zhang et al., 2015). Our hypothesis was based on the observations that LLPS driven by IDRs *in vitro* are thought to occur by weak electrostatic, dipolar interactions as well as interactions involving aromatic groups (reviewed in Brangwynne et al., 2015). Since these interactions are nonspecific, they are likely relatively promiscuous and could, in principle, occur between an IDR and other IDRs or with many other proteins. Moreover, even IDRs that have homotypic interactions based on local structural elements might be sensitive to other proteins and be most efficient at forming such specific assemblies only when concentrated by specific interactions (Xiang et al., 2015; Conicella et al., 2016). Thus, we asked whether IDR driven LLPS *in vitro* would be inhibited in the presence of other polypeptides, which would be analogous to the interior of the cell.

To test whether an IDR can promote LLPS in the presence of other proteins, we induced LLPS of either full-length hnRNPA1$_{\Delta hexa}$ or only the hnRNPA1$_{IDR}$ region (amino acids 186 to 300, **Figure 1A**) by dilution into lower salt (37 mM NaCl) (Lin et al., 2015) in the presence of increasing amounts of bovine serum albumin (BSA). We used the Δhexa-peptide variant of the

full-length hnRNPA1 protein as it is less prone to forming amyloid fibers during purification and analysis, and behaves similarly to the wild-type protein with regards to LLPS (Lin et al., 2015; Molliex et al., 2015). The fluorescently conjugatable SNAP tag was fused to both proteins to visualize droplets.

As the concentration of BSA increased, LLPS for both full-length SNAP-hnRNPA1$_{\Delta hexa}$ and the SNAP-hnRNPA1$_{IDR}$ was inhibited (**Figure 1B**). At higher BSA concentrations, we observed the formation of aggregated hnRNPA1$_{\Delta hexa}$ and hnRNPA1$_{IDR}$ that contrast with the liquid droplets seen in the absence of BSA (**Figure 1B**). As BSA concentrations increase, droplet sizes decrease and no large droplets form (**Figure 1C**). Interestingly, by looking at a subset of droplets of similar size across all BSA concentrations, we noticed that as BSA concentrations increased the intensities of hnRNPA1$_{\Delta hexa}$ droplets decreased (**Figure 1D**). The distribution of areas was approximately equal between samples (**Figure 1D inset**). The partition coefficient of LLPS (the ratio of protein within the concentrated phase versus within the dilute phase) is a measure of the equilibrium between the two states. Therefore, we interpret this decrease in intensity to mean that BSA shifts the phase separation equilibrium such that it is less favorable for hnRNP A1$_{\Delta hexa}$ to exist within the concentrated phase. At higher BSA concentrations the equilibrium shifts such that hnRNPA1$_{\Delta hexa}$ is below the critical concentration for LLPS. Thus, BSA is an inhibitor of LLPS driven by hnRNPA1 or its IDR alone under these conditions.

To determine if this inhibitory effect is unique to hnRNPA1 and BSA, we examined how BSA, lysozyme, and RNase A affected LLPS driven by the IDRs of hnRNPA1, FUS, or eIF4GII, all of

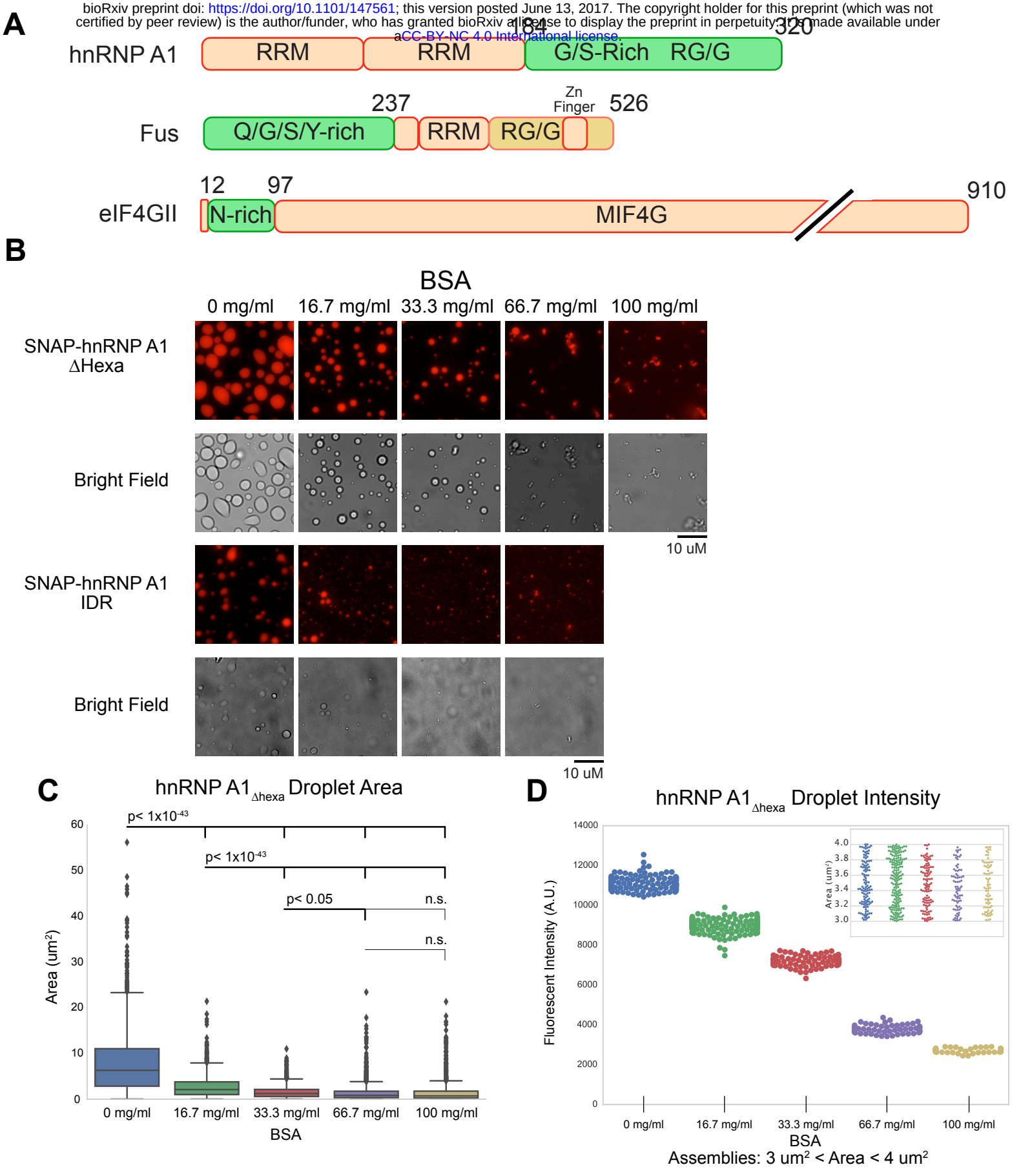

Figure 1. Competitor Proteins Disrupt IDR-Driven Phase Separations

(A) Domain structure of hnRNP A1, FUS, and eIF4GII

(B) Fluorescent and bright-field microscopy images of phase separated droplets formed at 37.5 mM NaCl by SNAP-hnRNP A1Δhexa and SNAP-hnRNP A1IDR with the indicated concentrations of BSA. Images are each independently scaled.

(C) Quantification of structure size for hnRNP A1Δhexa from (B), significance calculated with Welch's *t*-test for unequal size and variance.

(D) Quantification of the intensity of all structures between areas of 3 um and 4 um for hnRNP A1Δhexa from (B). These subsets of droplets have roughly equal distributions of size (inset)

158 which have been reported to undergo LLPS at low salt or low temperature (Lin et al., 2015;
159 Molliex et al., 2015; Patel et al, 2015). We observed that LLPS of FUS_{IDR} (amino acids 1-237),
160 $eIF4GII_{IDR}$ (amino acids 13-97), or the $hnRNPA1_{IDR}$ (184-320) (**Figure 1A)** were also inhibited by
161 the presence of BSA, lysozyme or RNase A **(Figure 2A)**.
162
163 To more closely mimic the cellular environment, we examined whether IDRs or IDR
164 containing proteins could undergo LLPS in the presence of yeast lysate, which had been
165 previously depleted of small metabolites and exchanged into droplet-forming buffer via
166 desalting columns. We observed that LLPS of $hnRNPA1_{\Delta hexa}$, $hnRNPA1_{IDR}$, and FUS IDR are all
167 strongly impaired in yeast lysates, which contained approximately 10 mg/ml protein (**Figure**
168 **2B**). Yeast lysates are our closest approximation of the cellular environment, and we find that
169 even lysates $1/10^{th}$ as concentrated as the cell (Milo, 2013) strongly impair LLPS of IDRs. Thus,
170 phase separation of multiple IDRs is sensitive to competition from other molecules within the
171 cell.
172
173 **Competitor proteins inhibit LLPS *in vitro* by interacting with IDRs**
174
175 What is the mechanism by which competitor proteins inhibit IDR-driven LLPS *in vitro*?
176 One possibility is that BSA, lysozyme, and RNase A share some specific property or structural
177 feature that inhibits LLPS of these IDRs. This is unlikely as BSA, lysozyme, and RNase A are
178 structurally unrelated, and vary in size (66.4, 14.3, and 13.7 kDa respectively) and pI (5.3, 11.35,
179 and 9.6, respectively). A second possibility is that any crowding agent will inhibit LLPS under

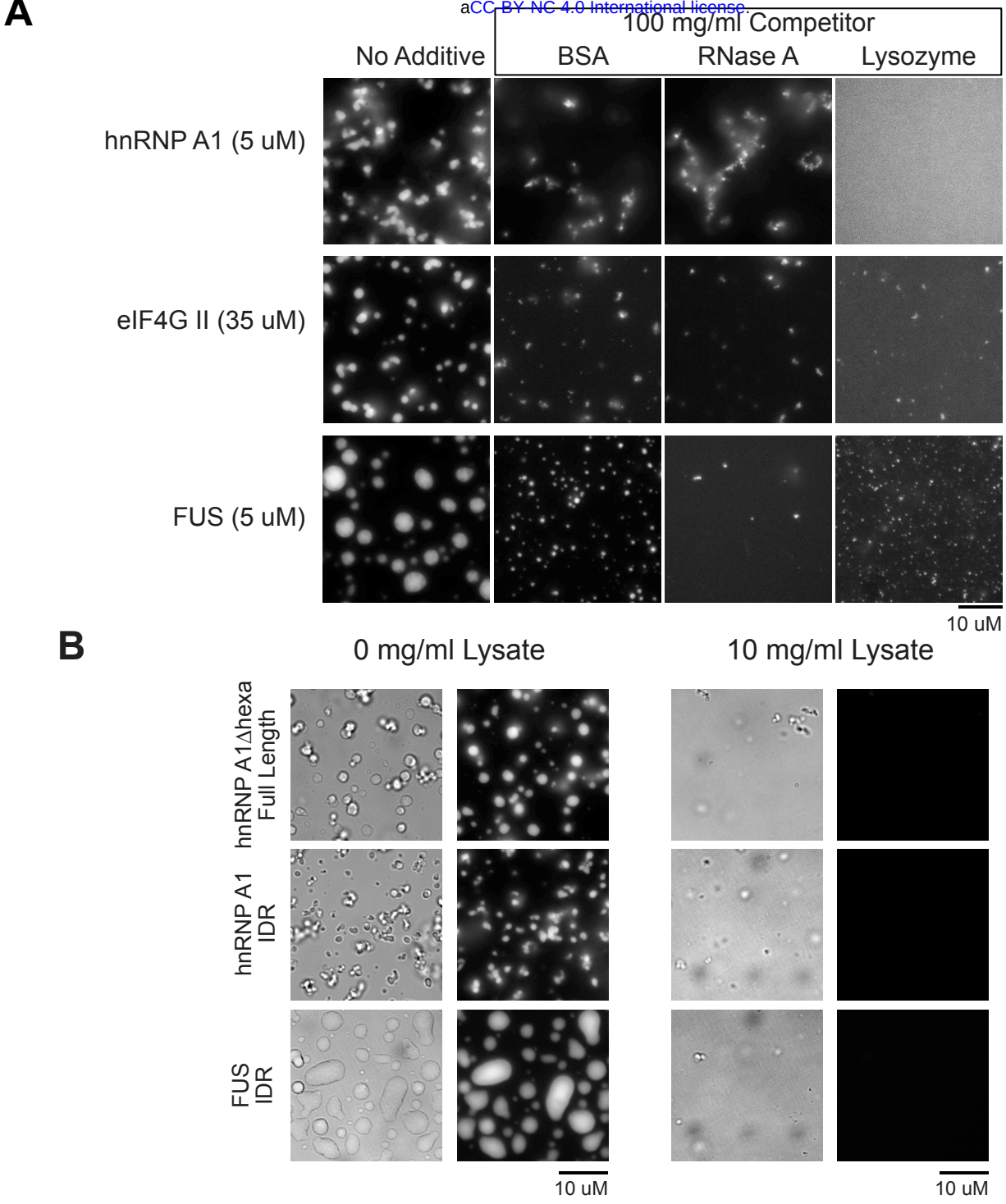

Figure 2. Globular Proteins Are Recruited to IDR-driven LLPS Droplets

(A) Fluorescent microscopy images of phase separated droplets formed at 37.5 mM NaCl by hnRNP $A1_{IDR}$, SNAP-FUS_{IDR}, and SNAP-$eIF4GII_{IDR}$ in the absence or presence of 100 mg/ml BSA, lysozyme, and RNase A.

(B) Fluorescent microscopy images of phase separated droplets formed at 37.5 mM NaCl by SNAP-hnRNP $A1_{\Delta hexa}$, hnRNP $A1_{IDR}$, and SNAP-FUS_{IDR}, in the absence or presence of approximately 10 mg/ml yeast lysate.

these conditions. However, we observe that LLPS driven by hnRNPA1$_{IDR}$ is stimulated by the crowding agents Ficoll and PEG, with phase separation occurring at higher ionic strengths and lower protein concentrations than without crowding agents **(Figure S1A)** (see also Lin et al., 2015; Molliex et al., 2015).

A third possibility is that these competitor proteins compete for promiscuous interactions between IDRs and thereby disrupt LLPS. A prediction of this model is that at low concentrations, insufficient to block LLPS, the competitor proteins would be recruited into the phase separated droplets (due to interactions with the IDR). To test this possibility, we examined the recruitment of fluorescent BSA or lysozyme into droplets formed by IDRs. At low concentrations both proteins were recruited to IDR-driven droplets without disrupting the assemblies. For example, at 500 nM concentration FITC-BSA was strongly enriched in droplets of hnRNPA1$_{\Delta hexa}$ **(Figure 3A)**. FITC-Lysozyme was also recruited (**Figure 3A**). Similarly, droplets of eIF4GII$_{IDR}$, hnRNPA1$_{IDR}$, and FUS$_{IDR}$ all recruited both FITC-BSA and FITC-lysozyme **(Figure 3B).** This suggests that these IDRs can interact with both BSA and lysozyme, consistent with the idea that competitor proteins could compete with the weak interactions that mediate LLPS.

The above evidence suggests that competitor proteins can interact with IDRs, both because these proteins are recruited into phase-separated droplets and because they inhibit LLPS at higher concentrations. Since these proteins were chosen at random and have diverse physical properties, and LLPS is also inhibited by metabolite-depleted cell lysates, we suggest that IDRs by themselves are likely to be susceptible to such nonspecific interactions in the more

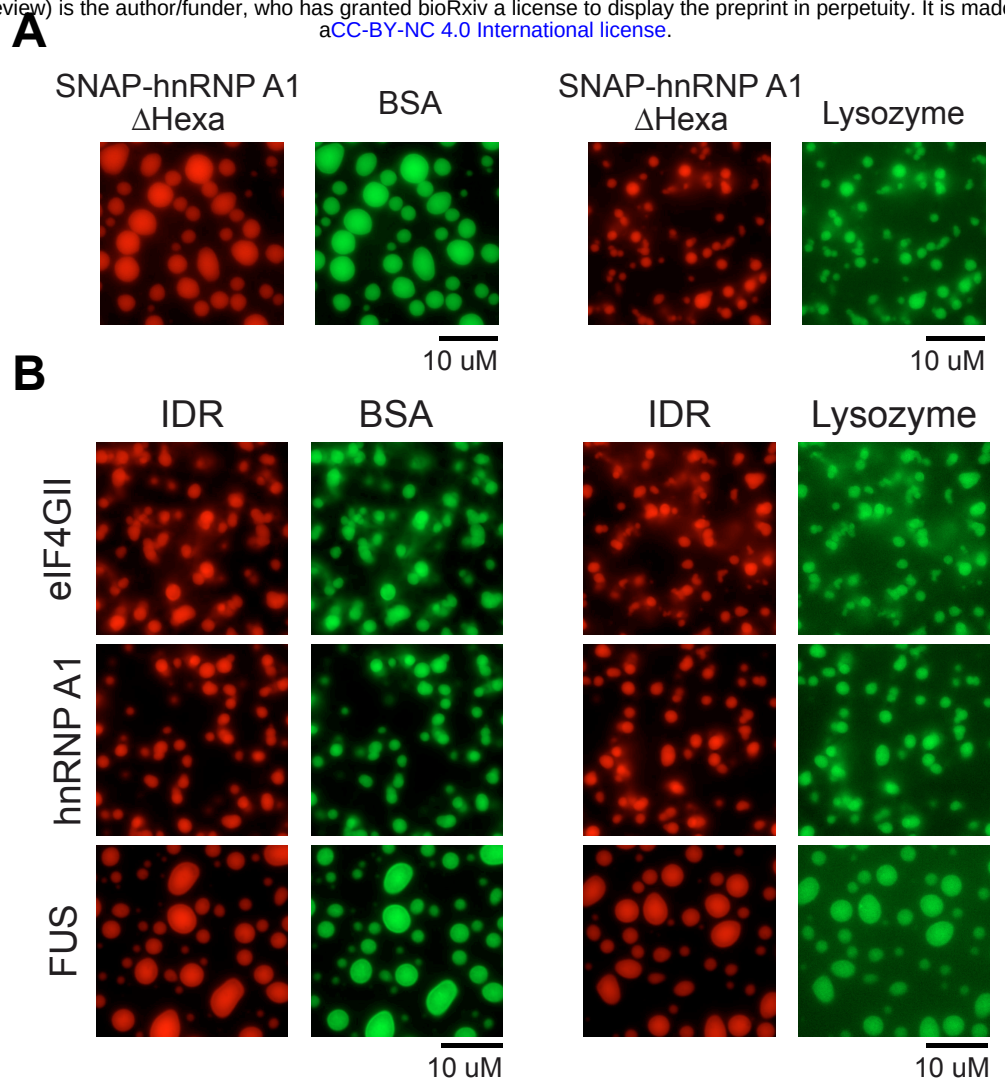

Figure 3. Globular Proteins Are Recruited to IDR-driven LLPS Droplets

(C) Fluorescence microscopy images of phase separated droplets formed at 37.5 mM NaCl by 25 uM SNAP-hnRNP A1$_{\Delta hexa}$ (red) and 500 nM FITC-labeled BSA (green) or FITC-labeled Lysozyme.

(D) Fluorescence microscopy images of phase separated droplets formed by SNAP-eIF4GII$_{IDR}$ (35 uM), SNAP-hnRNP A1$_{IDR}$ (5.25 uM), or SNAP-FUS$_{IDR}$ (5 uM) in the presence of either 10 nM FITC-BSA or 100 nM FITC-Lysozyme.

202 complex cellular environment. Therefore, in many cases, promiscuous interactions of IDRs are
203 unlikely to be sufficient for RNP granule assembly in cells.
204
205 **IDRs can enhance LLPS driven by specific interactions in the presence of competitor proteins**
206
207 The *in vitro* results above suggest that IDR-IDR interactions are susceptible to
208 competition by the complex protein mixture in the cell. However, IDRs are enriched in RNP
209 granule proteins (Decker et al., 2007; Jain et al., 2016; Kato et al., 2012; King et al., 2012; Reijns
210 et al., 2008), and IDRs can play a role in RNP granule assembly (e.g. Decker et al., 2007; Gilks et
211 al., 2004; Wang et al., 2014). In some cases, IDRs contain SLiMs that are important for assembly
212 of RNP granules (reviewed in Jonas and Izaurralde, 2013). However, since there are cases
213 wherein one IDR can functionally substitute for another in RNP granule assembly (Decker et al.,
214 2007; Gilks et al., 2004), a more generic role for IDRs in RNP granule assembly is also likely.
215
216 We hypothesized that IDRs in proteins that also make specific interactions could provide
217 promiscuous, nonspecific interactions that stabilize an RNP granule by acting together with the
218 specific interactions. By concentrating the IDRs through specific interactions, promiscuous IDR-
219 based interactions are biased to other components of the assembly. In this model, specific
220 interactions and nonspecific interactions both donate binding energy that promotes LLPS. This
221 model makes two predictions that we first tested *in vitro*.
222

First, the model predicts that LLPSs driven by specific interactions should be less susceptible to the interference from other competitor proteins, and may even be enhanced, given that high concentrations of such proteins can serve as crowding agents. Consistent with this view, we have shown that the LLPS driven by the specific interaction of an RNA binding protein, poly-pyrimidine tract binding protein (PTB), with RNA is promoted by BSA (Lin et al., 2015), an observation reproduced here. For example, while SNAP-tagged PTB and RNA showed limited assembly when mixed together at concentrations of 20 uM and 1.6 uM, respectively, the addition of 100 mg/ml BSA induced robust phase separation at these concentrations **(Figure 4A)**. Consistent with this effect being due to molecular crowding, the PTB-RNA LLPS is also stimulated by PEG or Ficoll, two additional crowding agents **(Figure 4A).** Thus, the specific PTB-RNA interactions are not outcompeted by BSA, allowing the crowding effect of BSA to dominate.

A second prediction of the model is that while IDRs alone are not sufficient to drive phase separation in the presence of competitor proteins, IDRs would contribute binding energy to phase separation driven by specific interactions, decreasing the threshold concentration of assembly. To test this prediction, we examined how IDRs affect PTB-RNA phase separation in the presence of competitor proteins. For example, 4 uM PTB and 0.32 uM RNA do not phase separate in 100 mg/ml BSA. However, we observed LLPS with identical concentrations of RNA and PTB, when the PTB was fused to either the FUS or Pub1 IDR **(Figure 4B)**. PTB fused to either IDR showed an increase in both the number and size of the assemblies visualized (**Figure 4C**). Therefore, weak interactions of IDRs can enhance phase separation in the presence of

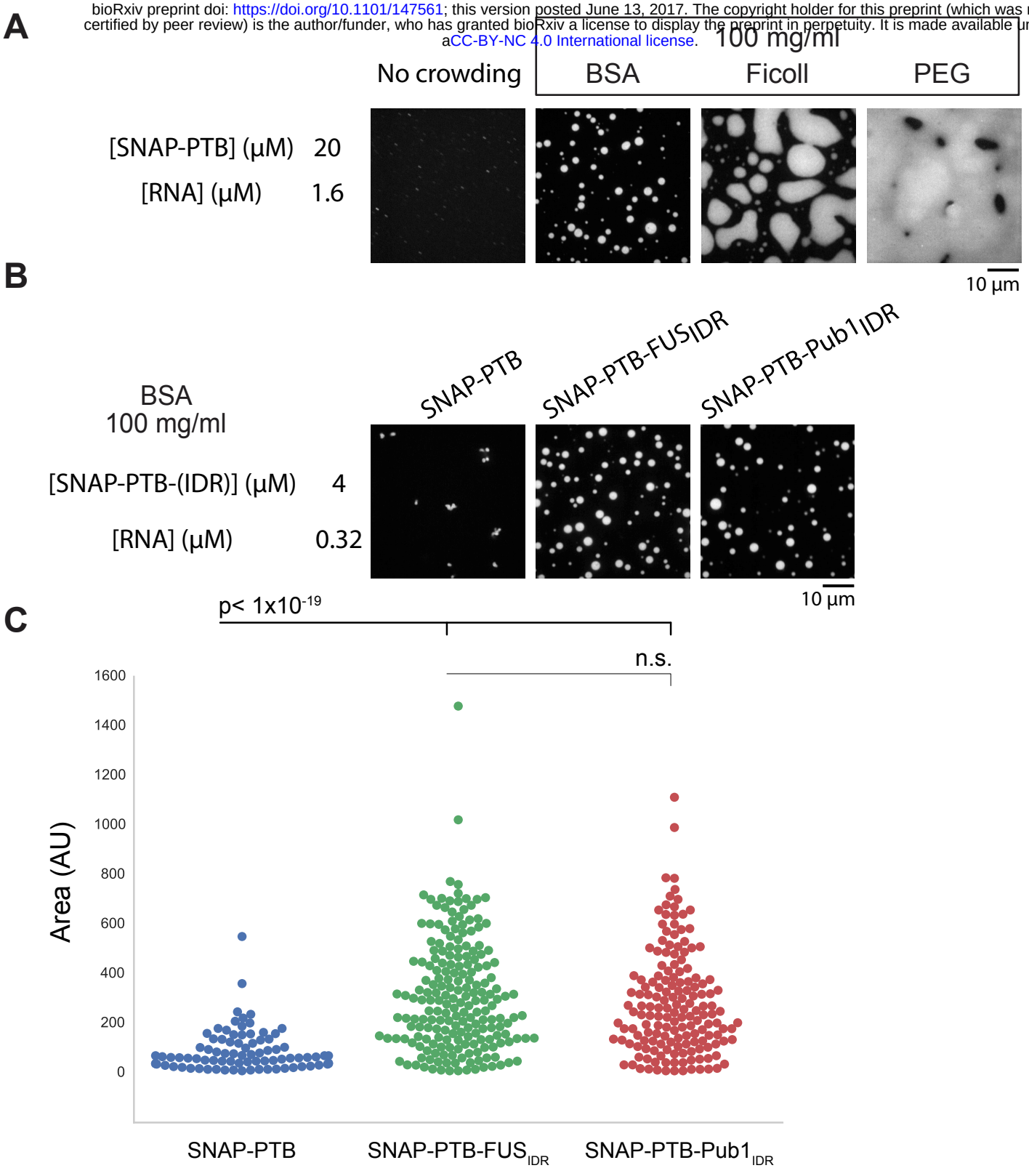

Figure 4. IDRs Enhance LLPS of PTB Plus RNA in the Presence of BSA

(A) Fluorescent microscopy images of phase separated droplets formed by SNAP-PTB and RNA in the presence or absence of 100 mg/ml BSA, Ficoll, or PEG.

(B) Fluorescent microscopy images of 4 uM SNAP-PTB, SNAP-PTB-FUS$_{IDR}$, or SNAP-PTB-Pub1$_{IDR}$ plus 0.32 uM RNA assemblies in the presence or absence of 100 mg/ml BSA.

(C) Quantification of assembly area for (B), with arbitrary units. Significance calculated with Welch's *t*-test for unequal size and variance.

245 competitor proteins, when present in molecules that also contain specific interactions which
246 are less susceptible to competition from cellular macromolecules.
247
248 **IDRs are often neither sufficient nor necessary *in vivo* to target components to RNP granules**
249
250 An assembly mechanism for RNP granules driven by specific interactions aided by
251 promiscuous interactions of IDRs has predictions for how components would be recruited to
252 RNP granules. Specifically, one would predict that generally IDRs would not be sufficient to
253 target a protein to an RNP granule, unless they contained a specific SLiM. Moreover, IDRs
254 would not be required for recruitment to a granule, although they could affect the partition
255 coefficient (the concentration of a component within versus outside of a granule).
256
257 To examine how IDRs of yeast proteins affect their targeting to P-bodies, we examined if
258 IDRs within Lsm4, Dhh1, Pop2, and Ccr4 **(Figure 5A**) were necessary and/or sufficient for their
259 recruitment into P-bodies. The IDRs of Lsm4, Dhh1, Pop2, and Ccr4 were fused separately to
260 either GFP or mCherry. IDR-fusion proteins were expressed in yeast co-expressing a
261 chromosomally GFP-tagged P-body component or containing a secondary plasmid containing a
262 mCherry tagged P-body component. P-bodies were induced by glucose deprivation for 15
263 minutes, and the percentage of P-bodies containing the IDR fusion protein was counted. For
264 example, clear enrichment in P-bodies was detectable for full length Lsm4 (**Figure 5B**).
265 However, the Lsm4 IDR was not sufficient for P-body localization **(Figure 5B)**. Similarly, the IDRs
266 of Dhh1, Pop2, and Ccr4, were insufficient for recruitment to P-bodies **(Figure 5C).** We then

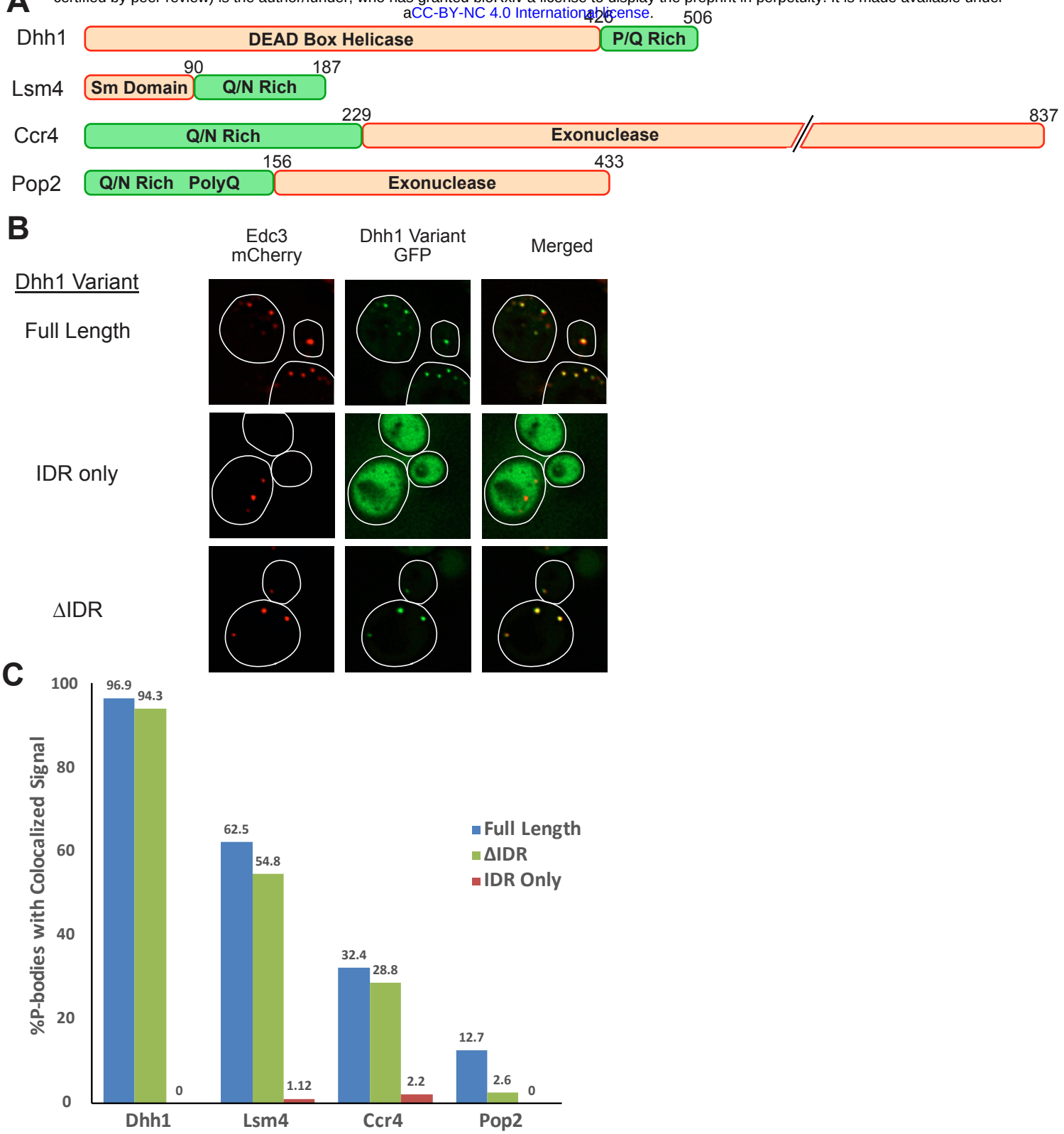

Figure 5. IDRs are neither sufficient nor required for P-body localization

(A) Domain structures of the yeast proteins Dhh1, Lsm4, Ccr4 and Pop2

(B) Dhh1-GFP variant fusions were expressed in Edc3-mCherry expressing yeast. After 10 minutes of glucose deprivation to induce P-bodies, cells were visualized by fluorescence microscopy. Representative images are presented.

(C) Quantification of the percentage of P-bodies that exhibited colocalization with the expressed fusion protein. GFP was fused to the N-terminus of Dhh1, Ccr4, and Pop2 variants. These variants were cotransformed with Edc3-mCherry. mCherry was fused to the C-terminus of the Lsm4 variants, which were expressed in cells encoding genomically-tagged Dcp2-GFP. Dhh1ΔIDR 1-427, Dhh1 IDR 427-506; Ccr4ΔIDR 148-837, Ccr4 IDR 1-229; Pop2ΔIDR 147-433, Pop2 IDR 1-156; Lsm4ΔIDR 1-90, Lsm4 IDR 91-187.

267 removed these IDRs from their full-length proteins, and found that deletion of the IDRs in Lsm4,
268 Dhh1, Ccr4 had little to no effect on their recruitment to P-bodies **(Figure 5B,C)**. However, for
269 the already poorly localized Pop2, deletion of the IDR did have a noticeable impact on
270 localization (Figure 5C). Thus, the IDRs of Lsm4, Dhh1, Ccr4, and Pop2 are not sufficient their
271 recruitment into P-bodies, but may contribute in cases where recruitment is already poor such
272 as Pop2.
273
274 **IDRs can enhance LLPS driven by specific interactions in cells**
275 The observations above suggest cellular assemblies such as RNP granules may form with
276 assembly primarily driven by a set of specific interactions, with the prevalence of IDR regions in
277 such assemblies contributing either a second set of promiscuous nonspecific interactions that
278 would enhance assembly, or having specific interactions with themselves that require high local
279 concentrations to form. Reported observations suggest, however, that some IDRs noticeably
280 contribute to RNP granule assembly in genetic backgrounds that limit assembly. One example
281 of this phenomenon is the previous observation that the C-terminal IDR of Lsm4 is not required
282 for P-body assembly normally, but plays a role in a strain lacking the P-body scaffold protein
283 Edc3 (Decker et al., 2007).
284
285 To determine if this may be a more general phenomenon, we examined how the C-
286 terminal IDR of the yeast Dhh1 protein promotes P-body formation. In *edc3Δ lsm4ΔC* yeast
287 strains, which lack visible P bodies, P-body formation can be partially rescued by the addition of
288 a single copy plasmid providing an extra copy of the Dhh1 gene, which through specific

289 interactions with RNA and Pat1 enhances P-body assembly (Rao et al., 2017, submitted).
290 Overexpression of Dhh1 in an *edc3Δ lsm4ΔC* background creates a cellular context where P-
291 bodies are just above the threshold for assembly. Dhh1 also has a C-terminal P/Q rich IDR
292 (**Figure 4**). To determine whether this C-terminal IDR contributes to P-body assembly, we
293 compared the ability of full length Dhh1 and a Dhh1ΔIDR truncation (1-427), which lacks the C-
294 terminal IDR (residues 428 to 506), to rescue P-body formation in an *edc3Δ lsm4ΔC* strain.
295
296 We found that wild-type Dhh1 rescues P-body formation in the *edc3Δ lsm4ΔC* strain, yet
297 the Dhh1ΔIDR variant fails to do so (**Figure 6A,B**), despite being expressed at levels similar to
298 the full-length protein **(Figure S2A)**. This demonstrates that the C-terminal IDR of Dhh1, while
299 not required for P-body formation normally, can contribute additional interactions that
300 enhance the formation of P-bodies when granule assembly is partially impaired.
301
302 In principle, the Dhh1-IDR could provide a specific interaction, perhaps containing a
303 SLiM, or a promiscuous interaction as we observed for several IDRs *in vitro*. If the Dhh1-IDR
304 makes a specific interaction, then it should not be functionally replaceable by other IDRs
305 capable of promiscuous interactions. Alternatively, if this IDR simply provides additional
306 promiscuous interactions then any IDR capable of such interactions should functionally replace
307 the Dhh1-IDR in promoting P-body assembly. To distinguish between these possibilities, we
308 determined whether the IDRs of human Lsm4, a P-body component, as well as the IDRs of two
309 human stress granule components, hnRNPA1, and the N-terminal domain of FUS, could replace
310 the function of the Dhh1 IDR. We also tested the disordered regions of two Late-Embryogenesis

311 Abundant (LEA) - like proteins, which are proposed to provide desiccation protection by
312 interacting promiscuously with proteins in the cell, potentially in lieu of water (Hand et al.,
313 2011). We utilized the IDRs of human proteins because these are very unlikely to contain
314 specific binding partners in yeast.
315
316 All three granule-component IDRs complemented the P-body assembly defect seen in
317 the Dhh1-ΔIDR construct (**Figure 6B**). Additionally, 2 LEA-like protein (LEA Group 3 – like from
318 the brine shrimp *Artemia franciscana,* "LEA-G3," and LEA Group2 – like from the nematode
319 *Steinernema carpocapsae*, "LEA-SC") IDRs also rescued the assembly defect (**Figure 6C**).
320 Addition of these IDRs does not cause appreciable assembly of large structures without glucose
321 deprivation (**Figure S2B**), demonstrating these assemblies are indeed P-bodies and not a
322 different constitutive aggregate. These results argue that the Dhh1 IDR does not provide a
323 specific interaction necessary for P-body assembly, as it can be replaced with a variety of other
324 human IDRs. This result also demonstrates that multiple different IDRs can complement the
325 Dhh1ΔIDR, consistent with promiscuous, nonspecific interactions of the IDRs contributing to
326 RNP granule assembly in conjunction with specific interactions.
327
328

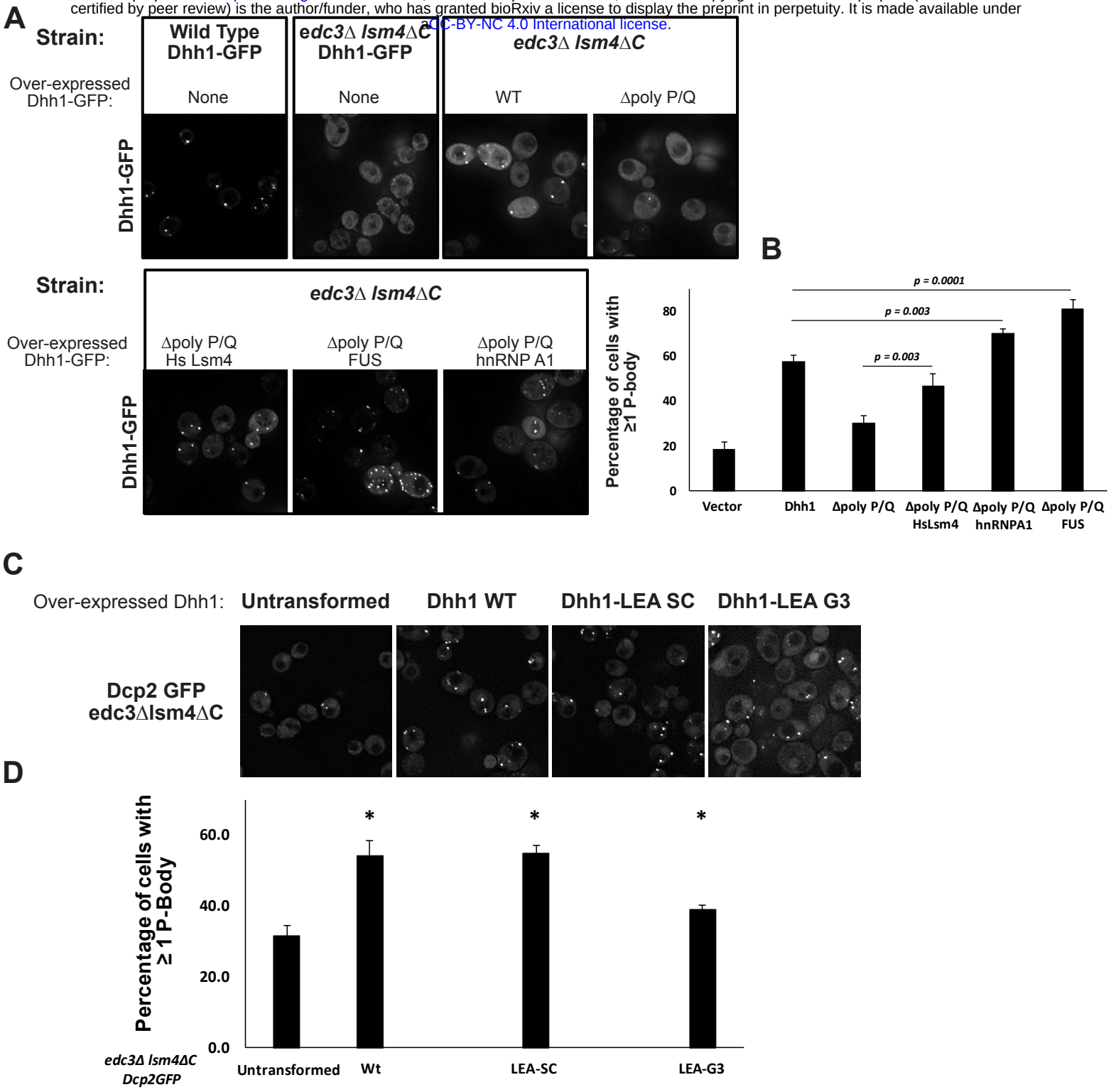

Figure 6. Specific interactions can synergize with promiscuous nonspecific interactions to drive assembly

(A) Fluorescent microscopy images of cells expressing Dhh1-GFP, either genomically or as a plasmid-expressed Dhh1-GFP variant. Cells were deprived of glucose for 10 minutes to induced P-body assembly.

(B) Quantification of (A), depicting the percentage of cells containing at least one P-body. (Student's *t*-test)

(C) Fluorescent microscopy images of cells expressing Dhh1 – LEA variants or wild-type Dhh1. Cells were deprived of glucose for 10 minutes to induced P-body assembly, and visualized by genomically GFP-tagged Dcp2.

(D) Quantification of (C), depicting the percentage of cells containing at least one P-body. (Student's *t*-test, * p<0.05)

DISCUSSION

RNP granules are cytoplasmic assemblies composed of specific groups of cellular proteins and RNA molecules (Jain et al., 2016, Khong et al., 2017 in submission). In principle, a specific assembly could be assembled in three manners: a) solely a set of specific interactions with well defined, and limited binding partners; b) through a summation of promiscuous interactions, where the sum of this network of interactions for a given molecule would bias its assembly characteristics, or c) through a combination of specific and promiscuous interactions. This third potential mechanism is supported by genetic analyses of the interactions that drive RNP granule assembly as well as our own findings. Specific interactions can clearly be important for assembly. For example, Edc3 dimerization via its YjeF-N domain is important for P-body assembly in yeast (Decker et al., 2007). G3BP dimerization, as well as interactions with caprin, are important for mammalian stress granule assembly (Tourriere et al., 2003; Kedersha et al., 2016). Some specific interactions can involve SLiMs found in IDRs that specifically interact with well-folded domains of other RNA binding proteins (reviewed in Jonas and Izaurralde, 2013). One example of this phenomena is the disruption of Edc3 localization to P-bodies in yeast caused by deletion of or interference with specific SLiMs in Dcp2's C-terminal IDR, which interact with a surface of Edc3 (Fromm et al., 2012, 2014). Thus, specific interactions between RNA binding proteins play important roles in formation of P bodies and recruitment of molecules into them. However, we have also shown that promiscuous interactions can play a role in assembly.

A key contribution of this work is to provide evidence that at least some IDRs function to promote RNP granule assembly both in cells, and in model biochemical systems, through weak interactions that require being coupled to protein domains with specific interactions. First, examination of the FUS, hnRNPA1, and eIF4GII IDRs reveal that they all interact nonspecifically with generic proteins, and those proteins and yeast lysates disrupt their ability to undergo LLPS in isolation (**Figure 1&2**). However, when tethered to the PTB RNA binding protein, which phase separates in the presence of RNA, promiscuous IDRs can promote LLPS, even in the presence of competitor proteins (**Figure 4**). Third, the C-terminal P/Q rich IDR of Dhh1 promotes P-body assembly in yeast, and this domain can be replaced by the IDRs of human Lsm4, hnRNPA1, or FUS, or by specific LEA proteins from brine shrimp or nematodes (**Figure 6**). The contribution of such IDRs to assembly is likely due to the ability of IDRs to promote LLPS through a variety of weak promiscuous interactions including electrostatic, cation-π, dipole-dipole and π-π stacking interactions (Brangwynne et al., 2015; Nott et al., 2015), which would be enhanced through effects analogous to avidity by coupled specific interactions of adjacent domains (Jencks, 1981).

Additional evidence exists that LLPS can be driven by combined specific and non-specific interactions. For example, even very high expression levels of hnRNPA1-Cry2 or DDX4-Cry2 fusion proteins do not phase separate in cells, unless the Cry2 protein is first triggered to assemble through specific light activated interactions (See Figure 2B&C of Shin et al., 2016). This observation highlights how specific oligomerization domains can act cooperatively with IDRs to promote LLPS in cells, and how some IDRs may be insufficient to undergo LLPS without additional oligomerization elements. As an example of the importance of non-specific

372 interactions in promoting cellular LLPS, the C-terminal IDR of yeast Lsm4 can enhance yeast P-
373 body formation, but it can be functionally replaced in this role by other IDRs (Decker et al.,
374 2007). Moreover, polyQ rich tracts, which are disordered IDRs capable of diverse interactions,
375 are prevalent in P-body components and RNA binding proteins (Decker et al., 2007; Reijns et al.,
376 2008), and can function in RNP granule assembly in *A. gossypii* (Lee et al., 2015). Taken
377 together, we suggest that many IDRs on RNA binding proteins provide an additional layer of
378 nonspecific interactions, and those interactions can contribute to granule formation when they
379 synergize with more specific interactions to stabilize the macroscopic structure.
380
381 An important point is that, even when insufficient in themselves to promote LLPS,
382 promiscuous IDRs can decrease the critical concentration for phase separation driven by more
383 specific interactions. We demonstrate this phenomenon for phase separation of PTB and RNA
384 *in vitro* (**Figure 4**), and for P-body assembly *in vivo* (**Figure 6**). This highlights that in a phase
385 diagram describing an assembly based on specific and promiscuous interactions, the addition of
386 promiscuous interactions can shift the system from an unassembled state to an assembled
387 state (**Figure 7A,B**).
388
389 Not all IDRs will influence RNP granule formation in the same molecular manner. Some
390 IDRs will provide specific interactions through SLiMs (Jonas and Izaurralde, 2013). Some IDRs
391 may also afford interaction specificity through formation of local structure, including amyloid-
392 like cross-beta interactions, that could be important in biological contexts where RNP granules
393 need to be long-lived or mechanically stable (Boke and Mitchison, 2017; Kato et al., 2012) or α-

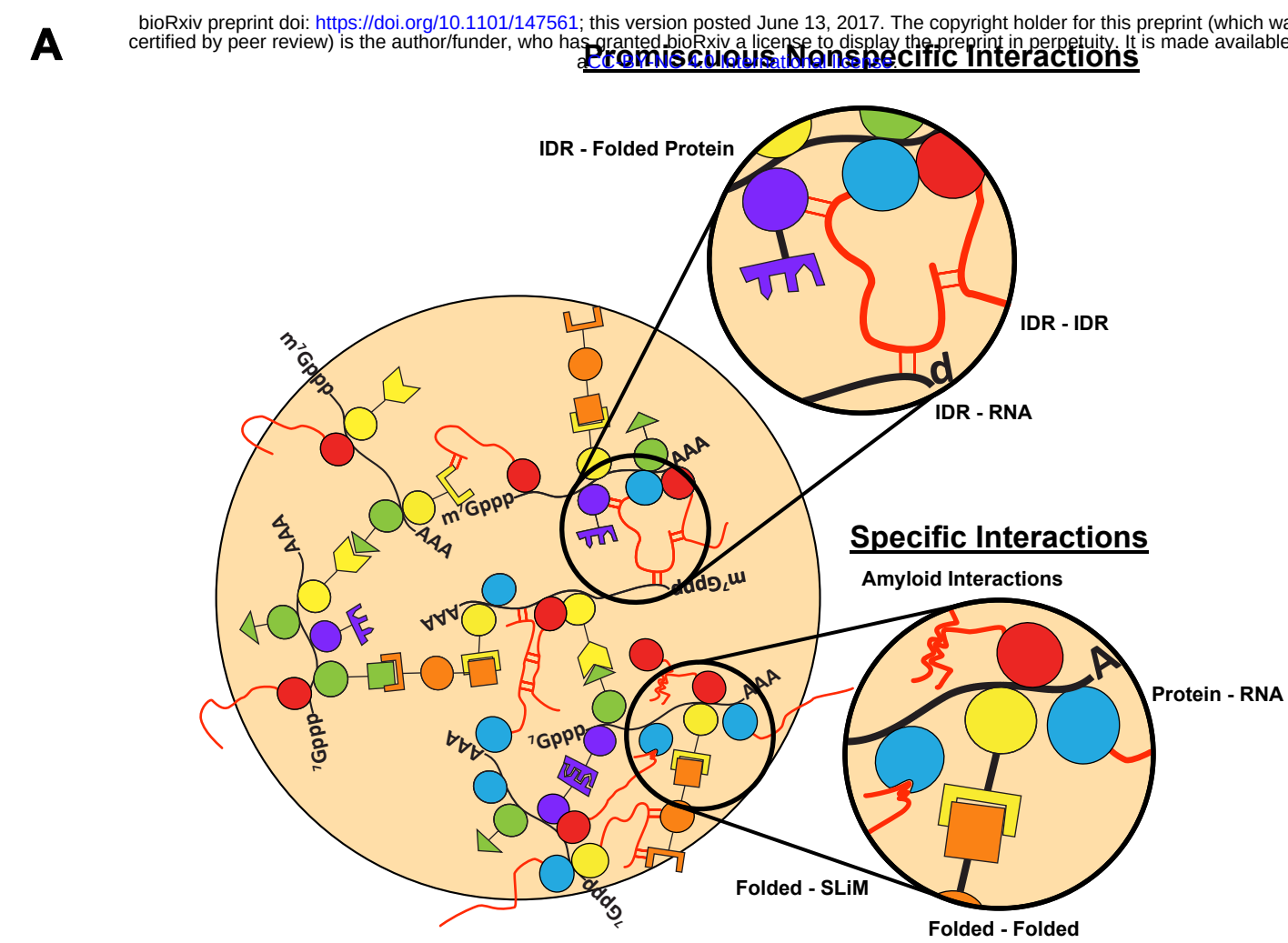

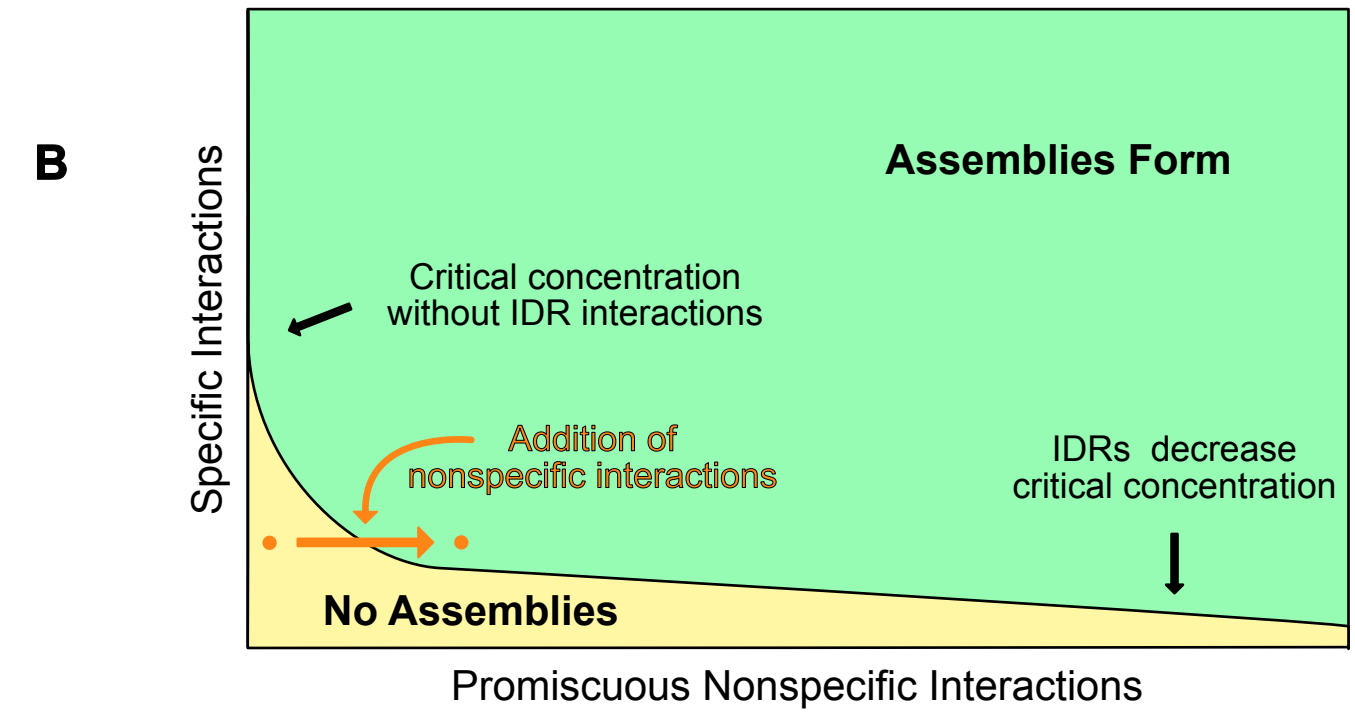

Figure 7. Model of RNP granule assembly and contributions of IDRs

(A) RNP granules assembly by a wide variety of specific and nonspecific interactions.

(B) A theoretical phase diagram depicting how the addition of nonspecific, IDR-driven interactions could decrease the critical concentration of assembly for higher-order structures.

394 helices (Conicella et al., 2016), both of which should show some sequence specificity. Charge
395 patterning can also afford sequence specificity, although likely to a lower degree (Nott et al.,
396 2015; Pak et al., 2016). Finally, as suggested here, some IDRs will provide promiscuous
397 interactions that can enhance RNP granule assembly. Therefore, interactions undergone by any
398 individual IDR that can contribute to intracellular LLPS likely lay on a scale from low affinity and
399 highly promiscuous, to moderate affinity and selective.
400
401 *A priori*, there are three general classes of promiscuous interactions that IDRs could
402 contribute to granule assembly. First, IDRs could interact with themselves or with other IDRs
403 through weak interactions, which is suggested by observations that both IDR-based hydrogels
404 and phase separated liquid droplets can recruit proteins with different IDRs (Kato et al., 2012;
405 Lin et al., 2015). Second, IDRs could have promiscuous interactions with RNAs, which is
406 suggested by observations that some IDRs cross-link to RNA *in vivo* (Castello et al., 2016) and
407 some IDRs bind RNA *in vitro* (Lin et al., 2015; Molliex et al., 2015). Finally, IDRs could make
408 promiscuous interactions with other well-folded domains of granule components. Note that
409 promiscuous interactions of IDRs with well-folded domains of proteins could provide an
410 evolutionary starting point for the formation of SLiMs, which are often found in IDRs. An
411 important future goal will be in determining how IDRs utilize each of these interaction types to
412 contribution to granule formation.
413
414 Utilizing promiscuous nonspecific interactions of IDRs to modulate the assembly of
415 macro-scale complexes has unique advantages. First, since such nonspecific interactions are not

limited to defined components or stereospecific arrangements, they can interact promiscuously with any number of individual components to enhance assembly. For example, in RNP granules, a diversity of mRNPs with different RNA binding proteins can be components of the granule. Promiscuous IDRs on RNA-binding proteins could interact with any of these mRNPs to enhance granule assembly. Moreover, IDRs can be subject to rapid evolution, and control by post-translational modifications, thus making them ideal components to change granule assembly parameters under selective pressure and in response to signaling pathways. Finally, we note that because higher-order assemblies are large with respect to a single IDR, promiscuous interactions of IDRs will mostly occur within the quinary space of the assembly, rather than with proteins outside of the assembly. This makes large assemblies particularly well suited to enhancement by IDRs.

Macromolecular assembly and concomitant LLPS mediated by combinations of specific and promiscuous interactions is a general mechanism for forming dynamic, meso-scale structures in eukaryotic cells. Eukaryotic cells contain many such assemblies including RNP granules, signaling complexes, DNA damage repair foci, and transcription complexes. It is notable that components of all of these assemblies are enriched in IDRs (Banani et al., 2016; Hegde et al., 2010; Hnisz et al., 2017; Iakoucheva et al., 2002; Kai, 2016; Minezaki et al., 2006). Thus, we suggest that higher order complexes will often be assembled by a combination of specific interactions that drive assembly, reinforced by a network of promiscuous nonspecific IDR based interactions, which stabilize the complex because of their physical coupling to specific assembly components. Such assemblies will be easily modified over time via evolution,

438 or in a dynamic sense by signaling pathways and post-translational modification. This would
439 occur without having to change the underlying specific assembly interactions, thus allowing
440 both rapid evolution of and immediate control over intracellular assemblies.
441
442
443
444 Author Contributions:
445 D.S.W.P. designed and performed experiments, provided substantial intellectual input,
446 contributed to writing the paper, and edited the paper.
447 B.V.T. and B.R. designed and performed experiments, and edited the paper.
448 Y.L. designed and performed experiments, provided substantial intellectual input, and edited
449 the paper.
450 L.M. performed experiments.
451 M.K.R. Provided substantial intellectual input, assisted with experimental design, and edited the
452 paper.
453 R.P. provided substantial intellectual input, assisted with experimental design, contributed to
454 writing the paper, and edited the paper.
455

EXPERIMENTAL PROCEDURES

Protein Purification and Labeling

Proteins were expressed and purified as previously reported (Lin et al., 2015). Proteins were expressed from the pMal-c2 vector (NEB), except for full length hnRNPA1 and related mutants, which were cloned into a modified pet11a vector (Novagen). Proteins were expressed in *E. coli* BL21(DE3) and purified with Ni-NTA and/or amylose resin under standard conditions. SNAP-PTB-IDRs were further purified through a Superdex200 column (GE Healthcare). Proteins were fluorescently-labeled with SNAP-Surface 488 or SNAP-Surface 649 (NEB) according to the manufacturer's protocols. Unincorporated dye was removed using Zeba Spin Desalting Columns, 7K MWCO (Thermo Fisher). Proteins were concentrated using Amicon Ultra 10K MWCO centrifugal filters (Milipore) and aggregates removed by ultra-centrifugation at 4°C for 30' at 50K RPM in a Beckman-Coulter TLA 100.2 rotor.

Fluorescence Microscopy

All yeast experiments and all images of SNAP-IDR and SNAP-hnRNPA1 were acquired on a DeltaVision epi-fluorescence microscope, equipped with an SCMOS camera. All images of SNAP-PTB-IDR were acquired on a Leica-based spinning disk confocal microscope (EMCCD digital camera, ImagEM X2, Hamamatsu; confocal scanner unit, CSU-X1, Yokogawa).

Droplet Assembly

For SNAP-IDRs and SNAP-hnRNPA1 (~2% fluorescently labeled), droplet assembly was initiated by diluting solutions to 37.5 mM NaCl, 20 mM Tris pH 7.4, 1 mM DTT. For SNAP-PTB-IDRs,

proteins and RNA, $(UCUCUAAAAA)_5$, were mixed at the indicated concentrations (including 100 nM SNAP-PTB-IDRs labeled with SNAP-Surface 649) in 100 mM NaCl, 20 mM imidazole pH 7.0, 1 mM DTT, 10% glycerol. N-terminal purification tags of SNAP-hnRNPA1 were removed by HRV C3 protease (EMD Milipore) during the dye conjugation step (Lin et al., 2015). N-terminal MBP and C-terminal His tags of SNAP-IDRs and SNAP-PTB-IDRs were cleaved just prior to droplet assembly with TEV protease (Promega ProTEV). Reactions were performed in glass-bottom chambers passivated with 3% BSA. FITC-conjugated Lysozyme (Nanocs) and FITC-BSA (Thermo Fisher Scientific) were mixed with SNAP fusion proteins prior to droplet assembly at concentrations of 100 nM and 10 nM, respectively.

Droplet Quantification:

Images were analyzed in FIJI as follows. Images were imported, flattened with a maximal intensity projection when applicable (hnRNP A1Δhexa droplets), and then thresholded using either the Default method (hnRNP A1 Δhexa droplets) or the Otsu method (PTB droplets) ('Threshold'). Binary images were eroded ('Erode) once to remove single pixels, then dialated ('Dialate') once to return droplets to their original size. This was followed by watershedding ('Watershed') to separate proximal droplets. FIJIs 'Analyze Particles' was used to generate ROIs, which were used to measure the maximal intensity projection, generating area and mean intensity values for each assembly.

Microscopy and Quantification for P-body Colocalization

Cells were grown at 30°C to OD_{600} of 0.3-0.5 in minimal media with 2% glucose as a carbon source and with necessary amino acid dropout to maintain plasmids and express constructs (See Supplemental File "Strains Plasmids and Antibodies"). Cells were stressed by glucose deprivation for 15 minutes before cells were concentrated for immediate microscopic examination at room temperature. All images underwent deconvolution using DeltaVision's algorithm.

Images were quantified using FIJI. To optimize yeast colocalization accuracy, single plane images were used and analysis were done in a blind manner. P-bodies were identified using protein markers (either Dcp2-GFP, Edc3-mcherry). Corresponding enrichment of the construct within the P bodies was then assessed manually. Manual assessment was required due to differential strengths of cytoplasmic signals between cells arising from stochastic variation and/or potentially different copy numbers of plasmids between cells.

Growth and Microscopy of Dhh1 Variants

To test the effect of Dhh1-IDR chimera on P-body recovery in the edc3Δ lsm4ΔC yeast (Strain yRP2338), yeast were transformed with vector only or vectors containing GFP fusions of Dhh1 wt, Dhh1-1-427 and Dhh1-IDR chimera using standard yeast transformation protocols. Two individual transformants were selected as biological replicates. The replicates were grown overnight to saturation at 30 °C with shaking in SD-Ura media (minimal media), containing 2% dextrose. The saturated cultures were re-inoculated into fresh SD-Ura media and grown to OD = 0.4-0.5. The cells were pelleted and transferred to S-Ura media lacking dextrose and shaken at

520 30 °C for 10 min prior to microscopic analysis. For the unstressed conditions, the cells were
521 pelleted without glucose starvation.
522 Yeast were analyzed via fluorescence microscopy on the DeltaVision Elite microscope with a
523 100 X objective using a PCO Edge sCMOS camera. ≥2 images comprising of 9 Z-sections were
524 obtained for each replicate. Images were analyzed using Image J. Z-projections derived from
525 summation of the Z-sections with constant thresholding were used to count the number of
526 yeast cells with ≥1 GFP-positive granule, and the percentage of cells with at least 1 granule was
527 calculated.
528

529 **Plasmid construction**
530

531 The Dhh1-GFP gene fragment containing the Dhh1 promoter was PCR amplified using the
532 genomic DNA from the Dhh1-GFP yeast strain (yeast GFP collection) and BSR_DhhGFP416NF
533 and BSR_DhhGFP416NR primers. The Adh1 terminator fragment was clone using the primers
534 BSR_Adh1SacF and BSR_Adh1SacR. The Dhh1-GFP and Adh1 terminator fragments were
535 inserted sequentially into the XhoI and SacI digested pRS416 vector, respectively, via Infusion
536 cloning (Takara). The poly P/Q residues of Dhh1 (428-506 were deleted from the Dhh1-GFP
537 containing vector using primers, Dhh11-427F and Dhh11-427R via the Phusion mutagenesis
538 protocol (Thermo Fisher). Lastly, the intron-less IDR sequence for HsLsm4 was synthesized using
539 gBLOCK technology from IDT technologies. The IDRs were PCR amplified using primers,
540 BSR_427FUSF and BSR_427FUSR, BSR_427A1F and BSR_427A1R, BSR_427HsLsm4F and

541 BSR_427HsLsm4R, for FUS, hnRNPA1 and HsLsm4, respectively and cloned into the linearized

542 Dhh1-1-427-GFP vector using Infusion cloning.

543

544

Banani, S.F., Rice, A.M., Peeples, W.B., Lin, Y., Jain, S., Parker, R., and Rosen, M.K. (2016). Compositional Control of Phase-Separated Cellular Bodies. Cell *166*, 651–663.

Boke, E., and Mitchison, T.J. (2017). The balbiani body and the concept of physiological amyloids. Cell Cycle *16*, 153–154.

Brangwynne, C.P. (2013). Phase transitions and size scaling of membrane-less organelles. J. Cell Biol. *203*, 875–881.

Brangwynne, C.P., Eckmann, C.R., Courson, D.S., Rybarska, A., Hoege, C., Gharakhani, J., Jülicher, F., and Hyman, A.A. (2009). Germline P granules are liquid droplets that localize by controlled dissolution/condensation. Science *324*, 1729–1732.

Brangwynne, C.P., Tompa, P., and Pappu, R.V. (2015). Polymer physics of intracellular phase transitions. Nat. Phys. *11*, 899–904.

Castello, A., Fischer, B., Frese, C.K., Horos, R., Alleaume, A.-M., Foehr, S., Curk, T., Krijgsveld, J., and Hentze, M.W. (2016). Comprehensive Identification of RNA-Binding Domains in Human Cells. Mol. Cell *63*, 696–710.

Conicella, A.E., Zerze, G.H., Mittal, J., and Fawzi, N.L. (2016). ALS Mutations Disrupt Phase Separation Mediated by α-Helical Structure in the TDP-43 Low-Complexity C-Terminal Domain. Structure *24*, 1537–1549.

Decker, C.J., Teixeira, D., and Parker, R. (2007). Edc3p and a glutamine/asparagine-rich domain of Lsm4p function in processing body assembly in Saccharomyces cerevisiae. J. Cell Biol. *179*, 437–449.

Elbaum-Garfinkle, S., Kim, Y., Szczepaniak, K., Chen, C.C.-H., Eckmann, C.R., Myong, S., and Brangwynne, C.P. (2015). The disordered P granule protein LAF-1 drives phase separation into droplets with tunable viscosity and dynamics. Proc. Natl. Acad. Sci. *112*, 7189–7194.

Feric, M., Vaidya, N., Harmon, T.S., Mitrea, D.M., Zhu, L., Richardson, T.M., Kriwacki, R.W., Pappu, R.V., and Brangwynne, C.P. (2016). Coexisting Liquid Phases Underlie Nucleolar Subcompartments. Cell.

Fromm, S.A., Truffault, V., Kamenz, J., Braun, J.E., Hoffmann, N.A., Izaurralde, E., and Sprangers, R. (2012). The structural basis of Edc3-and Scd6-mediated activation of the Dcp1: Dcp2 mRNA decapping complex. EMBO J. *31*, 279–290.

576 Fromm, S.A., Kamenz, J., Nöldeke, E.R., Neu, A., Zocher, G., and Sprangers, R. (2014). In Vitro
577 Reconstitution of a Cellular Phase-Transition Process that Involves the mRNA Decapping
578 Machinery. Angew. Chem. Int. Ed. *53*, 7354–7359.

579 Gilks, N., Kedersha, N., Ayodele, M., Shen, L., Stoecklin, G., Dember, L.M., and Anderson, P.
580 (2004). Stress granule assembly is mediated by prion-like aggregation of TIA-1. Mol. Biol. Cell
581 *15*, 5383–5398.

582 Hand, S.C., Menze, M.A., Toner, M., Boswell, L., and Moore, D. (2011). LEA Proteins During
583 Water Stress: Not Just for Plants Anymore. Annu. Rev. Physiol. *73*, 115–134.

584 Hegde, M.L., Hazra, T.K., and Mitra, S. (2010). Functions of disordered regions in mammalian
585 early base excision repair proteins. Cell. Mol. Life Sci. *67*, 3573–3587.

586 Hennig, S., Kong, G., Mannen, T., Sadowska, A., Kobelke, S., Blythe, A., Knott, G.J., Iyer, K.S., Ho,
587 D., Newcombe, E.A., et al. (2015). Prion-like domains in RNA binding proteins are essential for
588 building subnuclear paraspeckles. J. Cell Biol. *210*, 529–539.

589 Hnisz, D., Shrinivas, K., Young, R.A., Chakraborty, A.K., and Sharp, P.A. (2017). A Phase
590 Separation Model for Transcriptional Control. Cell *169*, 13–23.

591 Iakoucheva, L.M., Brown, C.J., Lawson, J.D., Obradović, Z., and Dunker, A.K. (2002). Intrinsic
592 Disorder in Cell-signaling and Cancer-associated Proteins. J. Mol. Biol. *323*, 573–584.

593 Jain, S., Wheeler, J.R., Walters, R.W., Agrawal, A., Barsic, A., and Parker, R. (2016). ATPase-
594 Modulated Stress Granules Contain a Diverse Proteome and Substructure. Cell.

595 Jencks, W.P. (1981). On the attribution and additivity of binding energies. Proc. Natl. Acad. Sci.
596 *78*, 4046–4050.

597 Jonas, S., and Izaurralde, E. (2013). The role of disordered protein regions in the assembly of
598 decapping complexes and RNP granules. Genes Dev. *27*, 2628–2641.

599 Kai, M. (2016). Roles of RNA-Binding Proteins in DNA Damage Response. Int. J. Mol. Sci. *17*, 310.

600 Kaiser, T.E., Intine, R.V., and Dundr, M. (2008). De Novo Formation of a Subnuclear Body.
601 Science *322*, 1713–1717.

602 Kato, M., Han, T.W., Xie, S., Shi, K., Du, X., Wu, L.C., Mirzaei, H., Goldsmith, E.J., Longgood, J.,
603 Pei, J., et al. (2012). Cell-free Formation of RNA Granules: Low Complexity Sequence Domains
604 Form Dynamic Fibers within Hydrogels. Cell *149*, 753–767.

605 Kedersha, N., Ivanov, P., and Anderson, P. (2013). Stress granules and cell signaling: more than
606 just a passing phase? Trends Biochem. Sci. *38*, 494–506.

607 Kedersha, N., Panas, M.D., Achorn, C.A., Lyons, S., Tisdale, S., Hickman, T., Thomas, M.,
608 Lieberman, J., McInerney, G.M., Ivanov, P., et al. (2016). G3BP–Caprin1–USP10 complexes
609 mediate stress granule condensation and associate with 40S subunits. J. Cell Biol. *212*, 845–860.

610 Kim, H.J., Kim, N.C., Wang, Y.-D., Scarborough, E.A., Moore, J., Diaz, Z., MacLea, K.S., Freibaum,
611 B., Li, S., Molliex, A., et al. (2014). Mutations in prion-like domains in hnRNPA2B1 and hnRNPA1
612 cause multisystem proteinopathy and ALS. Nature *495*, 467–473.

613 King, O.D., Gitler, A.D., and Shorter, J. (2012). The tip of the iceberg: RNA-binding proteins with
614 prion-like domains in neurodegenerative disease. Brain Res. *1462*, 61–80.

615 Lee, C., Occhipinti, P., and Gladfelter, A.S. (2015). PolyQ-dependent RNA–protein assemblies
616 control symmetry breaking. J. Cell Biol. *208*, 533–544.

617 Li, P., Banjade, S., Cheng, H.-C., Kim, S., Chen, B., Guo, L., Llaguno, M., Hollingsworth, J.V., King,
618 D.S., Banani, S.F., et al. (2013). Phase transitions in the assembly of multivalent signalling
619 proteins. Nature *483*, 336–340.

620 Lin, Y., Protter, D.S.W., Rosen, M.K., and Parker, R. (2015). Formation and Maturation of Phase-
621 Separated Liquid Droplets by RNA-Binding Proteins. Mol. Cell *60*, 208–219.

622 Lin, Y.-H., Forman-Kay, J.D., and Chan, H.S. (2016). Sequence-Specific Polyampholyte Phase
623 Separation in Membraneless Organelles. Phys. Rev. Lett. *117*.

624 Ling, S.H.M., Decker, C.J., Walsh, M.A., She, M., Parker, R., and Song, H. (2008). Crystal Structure
625 of Human Edc3 and Its Functional Implications. Mol. Cell. Biol. *28*, 5965–5976.

626 Lyons, S.M., Ricciardi, A.S., Guo, A.Y., Kambach, C., and Marzluff, W.F. (2014). The C-terminal
627 extension of Lsm4 interacts directly with the 3' end of the histone mRNP and is required for
628 efficient histone mRNA degradation. RNA *20*, 88–102.

629 Mayeda, A., Munroe, S.H., Cáceres, J.F., and Krainer, A.R. (1994). Function of conserved
630 domains of hnRNP A1 and other hnRNP A/B proteins. EMBO J. *13*, 5483–5495.

631 Milo, R. (2013). What is the total number of protein molecules per cell volume? A call to rethink
632 some published values: Insights & Perspectives. BioEssays *35*, 1050–1055.

633 Minezaki, Y., Homma, K., Kinjo, A.R., and Nishikawa, K. (2006). Human Transcription Factors
634 Contain a High Fraction of Intrinsically Disordered Regions Essential for Transcriptional
635 Regulation. J. Mol. Biol. *359*, 1137–1149.

636 Mitrea, D.M., Cika, J.A., Guy, C.S., Ban, D., Banerjee, P.R., Stanley, C.B., Nourse, A., Deniz, A.A.,
637 and Kriwacki, R.W. (2016). Nucleophosmin integrates within the nucleolus via multi-modal
638 interactions with proteins displaying R-rich linear motifs and rRNA. Elife *5*, e13571.

639 Molliex, A., Temirov, J., Lee, J., Coughlin, M., Kanagaraj, A.P., Kim, H.J., Mittag, T., and Taylor,
640 J.P. (2015). Phase Separation by Low Complexity Domains Promotes Stress Granule Assembly
641 and Drives Pathological Fibrillization. Cell *163*, 123–133.

642 Nott, T.J., Petsalaki, E., Farber, P., Jervis, D., Fussner, E., Plochowietz, A., Craggs, T.D., Bazett-
643 Jones, D.P., Pawson, T., Forman-Kay, J.D., et al. (2015). Phase Transition of a Disordered Nuage
644 Protein Generates Environmentally Responsive Membraneless Organelles. Mol. Cell *57*, 936–
645 947.

646 Pak, C.W., Kosno, M., Holehouse, A.S., Padrick, S.B., Mittal, A., Ali, R., Yunus, A.A., Liu, D.R.,
647 Pappu, R.V., and Rosen, M.K. (2016). Sequence Determinants of Intracellular Phase Separation
648 by Complex Coacervation of a Disordered Protein. Mol. Cell *63*, 72–85.

649 Patel, A., Lee, H.O., Jawerth, L., Maharana, S., Jahnel, M., Hein, M.Y., Stoynov, S., Mahamid, J.,
650 Saha, S., Franzmann, T.M., et al. (2015). A Liquid-to-Solid Phase Transition of the ALS Protein
651 FUS Accelerated by Disease Mutation. Cell *162*, 1066–1077.

652 Reijns, M.A.M., Alexander, R.D., Spiller, M.P., and Beggs, J.D. (2008). A role for Q/N-rich
653 aggregation-prone regions in P-body localization. J. Cell Sci. *121*, 2463–2472.

654 Riback, J.A., Katanski, C.D., Kear-Scott, J.L., Pilipenko, E.V., Rojek, A.E., Sosnick, T.R., and
655 Drummond, D.A. (2017). Stress-Triggered Phase Separation Is an Adaptive, Evolutionarily Tuned
656 Response. Cell *168*, 1028–1040.e19.

657 Shin, Y., Berry, J., Pannucci, N., Haataja, M.P., Toettcher, J.E., and Brangwynne, C.P. (2016).
658 Spatiotemporal Control of Intracellular Phase Transitions Using Light-Activated optoDroplets.
659 Cell.

660 Smith, J., Calidas, D., Schmidt, H., Lu, T., Rasoloson, D., and Seydoux, G. (2016). Spatioal
661 patterning of P granules by RNA-induced phase separation of the intrinsically-disordered
662 protein MEG-3. eLife.

663 Spector, D.L. (2006). SnapShot: Cellular Bodies. Cell *127*, 1071.e1-1071.e2.

664 Tourriere, H. (2003). The RasGAP-associated endoribonuclease G3BP assembles stress granules.
665 J. Cell Biol. *160*, 823–831.

666 Weber, S.C., and Brangwynne, C.P. (2012). Getting RNA and protein in phase. Cell *149*, 1188–
667 1191.

668 Xiang, S., Kato, M., Wu, L.C., Lin, Y., Ding, M., Zhang, Y., Yu, Y., and McKnight, S.L. (2015). The LC
669 Domain of hnRNPA2 Adopts Similar Conformations in Hydrogel Polymers, Liquid-like Droplets,
670 and Nuclei. Cell *163*, 829–839.

671 Zhang, H., Elbaum-Garfinkle, S., Langdon, E.M., Taylor, N., Occhipinti, P., Bridges, A.A.,
672 Brangwynne, C.P., and Gladfelter, A.S. (2015). RNA Controls PolyQ Protein Phase Transitions.
673 Mol. Cell *60*, 220–230.

674

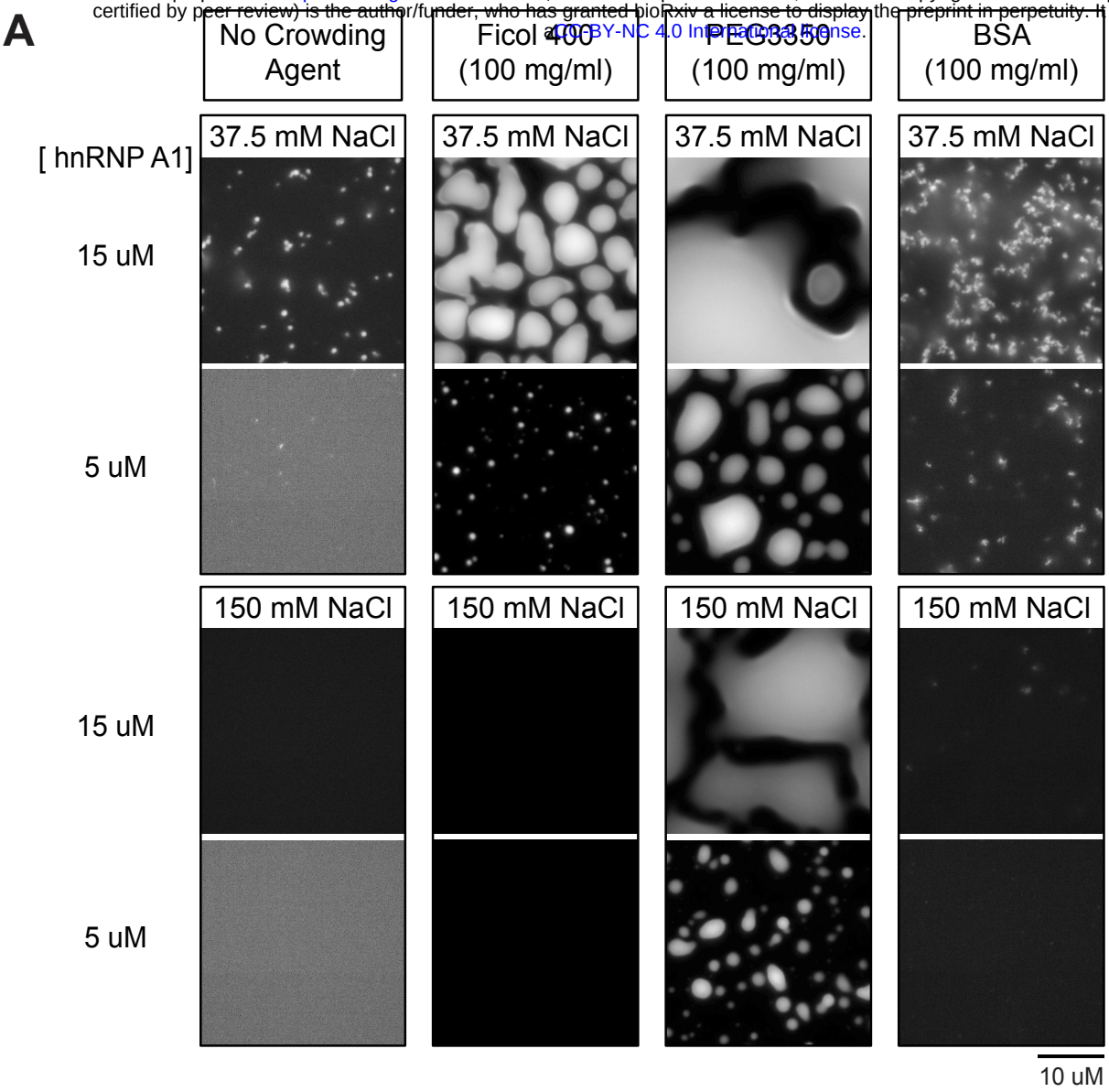

S1 Related to Figures 1 and 2: Diverse effects of crowding agents and proteins on LLPS

(A) Fluorescence microscope images of structures formed by SNAP-hnRNP A1 at either 150 mM NaCl or 37.5 mM NaCl in the absence or presence of 100 mg/ml Ficol 400, PEG 3350, or BSA. SNAP-hnRNP A1 concentrations were either 15 uM or 5 uM.

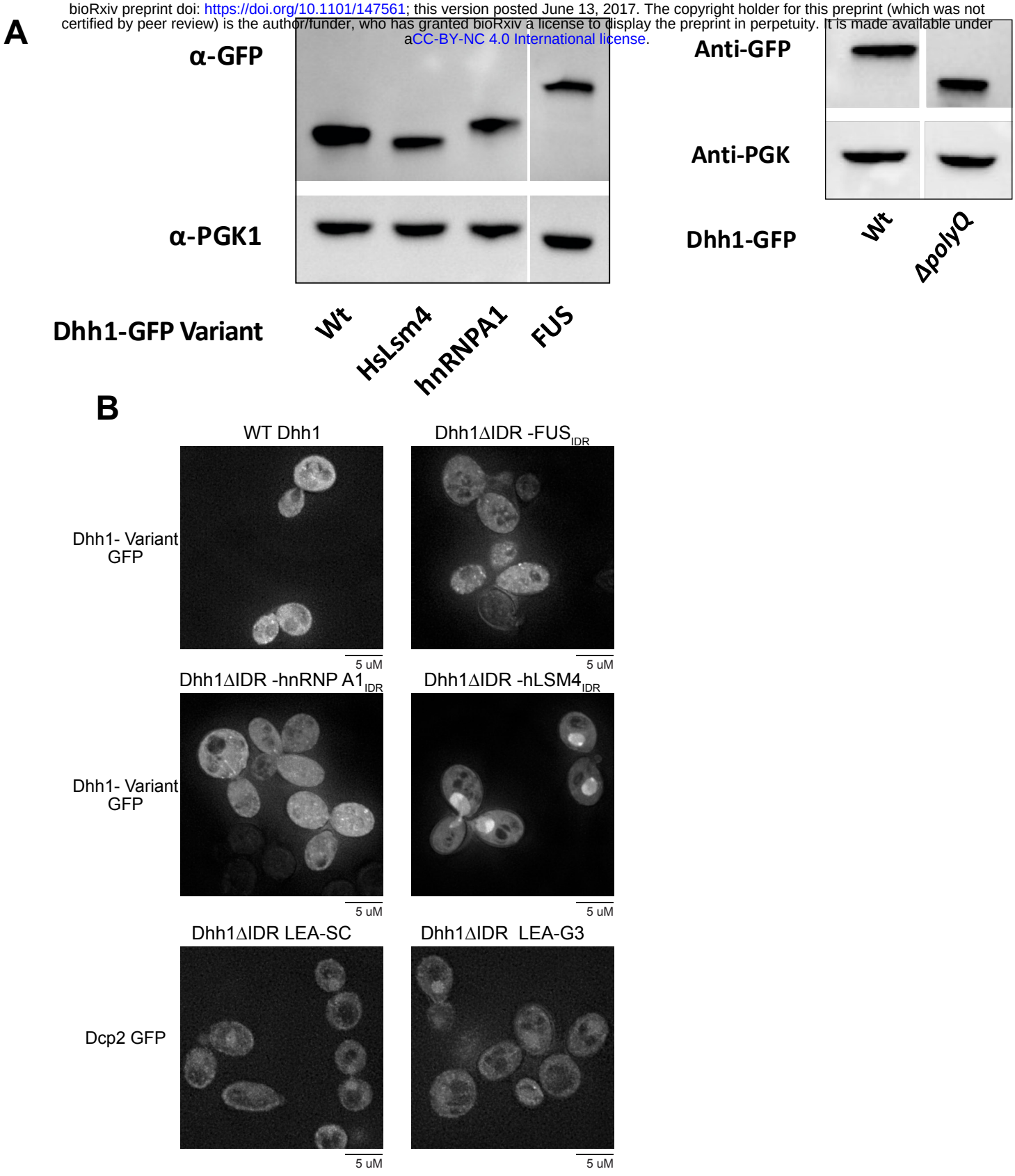

Sup 2 Related to Figure 6: Dhh1 IDR fusions do not form large assemblies in the absence of stress

(A) Western blot of Dhh1 variant expression

(B) Fluorescent microscopy images of cells expressing Dhh1-GFP, either genomically or as a plasmid-expressed Dhh1-GFP variant. Cells were growing under log phase growth conditions just prior to imaging.

Fig S2